A Composite Hydrogel for Brain Tissue Phantoms

Antonio E. Forte[*], Stefano Galvan, Francesco Manieri, Ferdinando Rodriguez y Baena,
Daniele Dini[*]

Department of Mechanical Engineering, Imperial College London, South Kensington Campus, Exhibition Road, London SW7 2AZ, UK

[*]*Corresponding Authors: antonio.forte10@imperial.ac.uk, d.dini@imperial.ac.uk*

Abstract

Synthetic phantoms are valuable tools for training, research and development in traditional and computer aided surgery, but complex organs, such as the brain, are difficult to replicate. Here, we present the development of a new composite hydrogel capable of mimicking the mechanical response of brain tissue under loading. Our results demonstrate how the combination of two different hydrogels, whose synergistic interaction results in a highly tunable blend, produces a hybrid material that closely matches the strongly dynamic and non-linear response of brain tissue. The new synthetic material is inexpensive, simple to prepare, and its constitutive components are both widely available and biocompatible. Our investigation of the properties of this engineered tissue, using both small scale testing and life-sized brain phantoms, shows that it is suitable for reproducing the brain shift phenomenon and brain tissue response to indentation and palpation.

Keywords

Composite Hydrogel, Tissue Phantom, Brain Tissue, Mechanical Characterization, Surrogate Material, Mimicking

Introduction

Surgeons are required to reach high standards and perform complex technical tasks in a short training period [1]. However, early in their career, trainees are not given the opportunity to operate on a sufficient number of patients, nor to perform an exhaustive mix of procedures. The reduction of assisted training hours in Europe (since 2009) and the USA (since 2011), along with a growing attention on patient safety [2], have further worsened this scenario. Cadaveric training is still considered the gold standard in order to achieve technical proficiency [3], as it provides details on the anatomical structures and their positions, practice on skin incisions and tactile feedback. However, an absence of specimens, ethical issues, and high costs of handling, storage and preservation of the tissue all contribute to offsetting the advantages of this method. Animal models are cost effective, and they are characterised by a certain degree of realism owing to the presence of soft tissue [4]. On the other hand, they are not free of drawbacks. For example, anatomic structures are often different from human specimens to an extent which depends on the combination of organs and animals. Ethical restrictions are also involved in the utilization of the samples, and specific equipment requirements must be met when handling and testing animal tissues.

Haptic virtual-reality simulators are used to overcome the drawbacks of animals and human specimens. Recent advances in computer graphics have made it possible to design simulators with a level of fidelity that makes it possible to reproduce real surgical environments. Simulations such as these may be used for training in minimally invasive procedures (MIP), such as laparoscopy and endoscopy, but their ability to accurately reproduce complex, dynamic interactions is questionable. Additionally these systems are expensive [5], the transfer of simulator-based skills to the real operating theatre remains doubtful [6, 7], and the number of procedures available for simulation-based training is limited.

Phantoms are reproductions of human parts and organs that allow a trainee to practice positioning of anatomical structures, as well as hand-eye coordination. In addition, the applicability of reliable synthetic organs extends well beyond training purposes, as they can be employed in, for example, prosthesis design, design and testing of robotic aided surgery systems, impact tests and traumatic

injury analysis. Furthermore, if the phantom material is biocompatible, it can be used for bio-implants [8-11] and tissue development [12-16]. In fact, in specific cases, cell differentiation and regeneration is promoted in scaffolds that exhibit mechanical properties similar to those of the real tissue [12-16]. Although the impact of successfully designing advanced bioengineered materials that are able to mimic the mechanical behaviour of native tissues is evident, this is not a straightforward task, especially when the aim is to reproduce the behaviour of organs.

Some human tissues, like the brain, present non-linear elastic mechanical responses, in addition to rate-dependent characteristics [17] (*i.e.* the tissue stiffness changes depending on the strain/displacement-rate). This behaviour is due to the interaction between the cerebrospinal fluid (CSF) and the solid matrix of the tissue, as well as the viscoelastic properties of the solid matrix itself [18]. For this reason, the brain deforms differently during trauma (fast rate), indentation and palpation (medium rate), and brain shift (slow rate) phenomena. In particular, brain shift is a non-rigid deformation occurring during surgical procedures when a craniotomy is performed. Due to changes in the boundary conditions, the brain starts to "shift" along the direction of gravity. The loss of CSF during surgery, and consequentially of buoyancy forces surrounding the brain, is recognised as the main cause of brain shift [19, 20]. It has been shown that brain can shift up to two centimetres in a non-rigid fashion [21]. This introduces a non-negligible error in target location, which would results in loss of accuracy if not accounted for. Conventional phantom materials are not designed to mimic such a complex response, and thus the research aimed at identifying suitable natural and synthetic compounds that are capable of achieving this task is of immediate significance.

A number of strategies and material candidates for brain phantom fabrication are available in the literature, although to-date the attention has been focused mainly on drug delivery and near-infrared spectroscopy [22-24]. In the last decade, synthetic materials such as Agarose gelatine, Sylgard 527 silicone gel, Hyaluronic Acid (HA) and Polyvinyl Alcohol (PVA) have been developed for soft tissue mimics; these recent efforts are briefly reviewed here. Cloyd et al. [25] analysed a composite gel produced with Agarose, Alginate and HA for human nucleus pulposus measuring compression peaks of about 4000 Pa at 0.05/s strain rate for 25% deformation; however, this value is considerably higher than the experimental results shown by Miller [17] for

porcine brain samples. De Lorenzo et al. [26] used Sylgard 527 (Dow Corning, USA) as synthetic surrogate of brain tissue, designing a brain phantom and evaluating the deformations predicted by their novel simulation algorithm. However, no experimental evidence was provided for the characterisation of the mechanical properties of the gel. The same gel was also used by Brands et al. [27] to compare its mechanical properties with the brain tissue. A rheometric analysis revealed that the gel exhibited linear viscoelastic behaviour for strains up to 0.5 and frequencies up to 460 Hz; this is far from capturing the established characteristics of brain tissue. Dumpuri et al. [20] used PVA at 7% concentration to validate the fidelity of their constrained linear inverse model but no detailed material studies are reported in their contribution in order to compare the mechanical properties and loading response of the synthetic material and brain tissue.

The present contribution focuses on the design of a brain phantom made of a novel composite hydrogel (CH) that can reproduce the dynamic mechanical response of brain tissue, providing an accurate mimicking of the organic tissue at different displacement rates and for different loading conditions. Taking advantage of the hybrid mechanical capabilities of binary polymer blends, we generate a novel porous composite hydrogel (see Methods for more details about the CH composition and fabrication). The strategy adopted by the authors relied on the identification of individual components whose properties could be combined to form a stable coupled network with porosity, elastic and viscoelastic properties representative of brain tissue. Testing and characterisation of a number of individual compounds led to the realisation of a superior construct obtained by combining the elastic characteristic of PVA and the viscoelastic response of Phytagel (PHY). The gel is simple to prepare and its components are widely available, inexpensive and biocompatible [28-33]. By means of molecular bindings a coupled binary network is synthesised [34], which guarantees that the mechanical characteristics of the synthetic material can be easily tuned. The result is a non-linear hyper-elastic, rate-dependent material suitable for reproducing the tissue dynamic mechanical behaviour, as demonstrated in the following section. The adaptability of the CH in terms of reproducing the mechanical response of brain tissue is also demonstrated by a further tuning process that allows the material to reproduce brain tissue cutting for surgical applications. Preliminary studies of the puncturing resistance of the CH have also been presented in [35].

Finally, we study the behaviour of a life-sized human brain-skull phantom, and describe its manufacturing process. This is the first synthetic replica of a human brain that provides an accurate reproduction of geometric features and a reliable dynamic response. Furthermore, the loss of CSF can be regulated by a dedicated draining system, enabling the experimental simulation of the brain shift phenomenon in a laboratory.

Methods

Sample preparation

PVA (146,000-186,000 molecular weight), PHY and deionised water were supplied by Sigma-Aldrich, USA. Sylgard 184 and 527 were provided by Dow Corning, USA. Gelatine powder was provided by Dr Oetker, Germany. All the concentrations in the following sections are expressed as a percentage by mass (wt %). Samples of porcine brain were provided by a local supplier within 24 hours post-mortem.

PHY is a high strength, water-soluble tetrasaccharide generically used as gelling agent in plant and microbiological culture. PHY powder (concentration 2.2%) was dissolved in deionised water under constant stirring. The solution was progressively heated to 90 °C, under which complete and homogeneous dispersion of the material was obtained after 30 min. The samples were stored at room temperature for 24 h before testing.

Gelatine gels are frequently used in the food industry to thicken and stabilise various products such as desserts, yogurts, candies and jellies. Gelatine gels were produced by mixing deionised water and beef gelatine in powder form at 90 °C for 5 minutes under vigorous stirring at 5 and 10% concentrations. The solution was then poured in Petri dishes and allowed to cool down to reach room temperature. Afterwards the samples were stored for 18h at 13 °C before testing.

PVA is a non-toxic, hydrophilic, synthetic polymer recently introduced in tissue engineering for its biocompatibility [36]. PVA was dissolved in deionised water at 90 °C for 1 h under vigorous stirring at 7 and 15%concentrations. The dissolving time normally varies with the concentration adopted. The solution was then poured in Petri dishes and allowed to cool down to room temperature. The samples were then stored for 18 h at -25 °C and subsequently thawed for 6 h before testing.

Sylgard 184 (also known as PDMS) is a silicone elastomer that has been extensively used as casting material for soft lithographic replications. The elastomeric part and curing agent were mixed together in a 10:1 ratio and cured at room temperature for 24h before being tested. Sylgard 527 is a silicone dielectric gel normally used for sealing and protecting electronic devices. Its two constituents (parts "A" and "B") were mixed together in 1:1 weight ratio and cured at 80 °C for 4 h. The gel was then left to cool down at room temperature before being tested.

The CH was obtained dissolving 6% PVA and 0.85% PHY separately in deionised water for 1 h at 90 °C resulting in different individual solutions. The two solutions were then mixed together in 1:1 weight ratio at 70 °C under constant stirring for 30 min. Particular care was used to avoid evaporation during the process. The solution was poured into Petri dishes, let slowly cool down and then frozen at -25 °C for 18 h. The samples were tested after 6 h thawing. Furthermore, additional samples at different concentrations were prepared for the SEM analysis keeping constant the PVA/PHY concentration ratio (PVA 4% + PHY 0.56% and PVA 8% + PHY 1.13%). A surgical trephine was used for cutting cylindrical shape from the gels stored in Petri dishes, to be used as compression tests samples (diameter 11 mm, height 7±1 mm). Large cylindrical CH samples were prepared for the indentation test protocol (diameter 100 mm, height 45±1 mm) and flat disk-shaped samples for the rheometric analysis (cylindrical sample dimensions: diameter 25 mm, height 2±0.5 mm). For each material, the samples were prepared from at least three different batches.

Mechanical characterization

The Mach-1™ mechanical testing system (Biomomentum, Canada) was chosen as testing rig for the compression tests since particularly recommended for soft material tests. A 1.5 N single-axis load cell with a resolution of 75 μN was used to measure the vertical force. The vertical displacement was measured by the moving stage of the rig with a resolution of 0.1 μm. With the aim of minimizing the contact friction polytetrafluoroethylene (PTFE) sheets were attached to the surfaces of the compression platens [17]. To avoid drying of the specimen during tests at low displacement rate a moist chamber was used. One loading cycle was executed on each specimen. Since the samples tended to adhere to the platen when coming into contact, the measured force

showed small contributions from adhesion effects. For this reason a protocol was developed using the "Find Contact" routine of the Biomomentum software to guarantee that the starting point of the tests was the same for all specimens. A spherical indenter (4 mm diameter) was mounted on the movable stage before placing the samples on the apparatus. The routine was programmed to initially move the indenter vertically (z axis) with a velocity of 0.01 mm/s and to stop as soon as a vertical force of 150 μN was measured by touching the lower platform of the rig. This point was set to be the zero for the z-axis of the rig. Then the gel specimen was placed on the fixed platform. Once again, the indenter was moved towards the specimen with a velocity of 0.01 mm/s and stopped as soon as a vertical force of 150 μN was measured by touching the sample. The z axis position was saved to correspond to the height of the current specimen. This procedure assured a precise measurement of the height of each specimen minimizing the adhesion (suction) effect that could have affected measurement of the initial size of the sample if using the flat platen. Finally the flat compression platen was mounted on the movable stage and brought to the corresponding height (previously recorded) of the specimen. In this position the specimen was left for about 1 minute before the actual test began. In order to detect the non-linear elastic response of the material the samples were compressed at constant velocity until a displacement corresponding to 30% of the measured height was achieved. Particular attention was used to monitor that samples had uniformly expanded in the radial direction and that their upper and lower faces remained adhered to the moving platen and the fixed platform for the entire duration of the test. The tests were conducted at two different velocities: 8.3×10^{-2} mm/s ("medium rate") and 8.3×10^{-4} mm/s ("slow rate"). At least 10 samples were tested for each velocity and for each synthetic material. The indentation test protocol was taken from Gefen et al. [37], who performed *in-vitro* indentation tests on brain tissue. The Biomomentum Mach 1 was also used for this testing protocol. To assure the same initial test conditions for all the specimens the "Find Contact" routine of the Biomomentum software was used as previously described. A 4 mm indenter was then pressed against the sample. Zheng et al. [38] recommended to use and indenter radius smaller than 25% of the sample thickness (45 mm in our case). Van Dommelen et al. [39] suggested that by indenting up to 10% of the sample thickness, the influence of sample height is not present. For this reason a constant

depth of penetration of 4 mm was used. The CH was indented at 3 and 1 mm/s (approximately 0.066 s-1 and 0.022 s-1 strain rates respectively, defined as the instantaneous displacement rate of the indenter divided by the instantaneous displacement [40]) and held for 90 s during which the contact force was continuously acquired at 100Hz and plotted over time. Each indentation was performed 6 times at each indentation site to acquire non-preconditioned (cycle 1) as well as preconditioned data measurements (cycles 5 and 6) as suggested by Gefen et al. [37]. A waiting programmed routine with 45 s delay between subsequent indentations was used to allow elastic recovery of the hydrogel [37]. Indentation test sites were ~5 mm away from each other so that a non-preconditioned area of the specimen could be indented for the first loading cycle. At least 6 tests (6 indentation cycles each) were performed for each indentation speed in order to obtain statistically representative data and calculate average and standard deviation.

A Discovery HR-1 Rheometer (TA Instruments, Germany) was used to measure the storage (G') and the loss (G'') moduli of CH and to Compare the results with available brain tissue data in the literature [41]. A plate-plate flat configuration was used (25 mm diameter) and sand paper was attached on the surface of the plates to prevent slipping. The top plate of the rheometer was slowly lowered until touching the top of the sample and measuring a maximum axial force of 0.01 N. A shear strain of 1% was applied on the upper plate varying the frequency from 0.01 to 25 Hertz (sweep frequency analysis). For higher frequencies the measurements were unreliable due to inertia effects. At least 10 tests were run for each material in order to calculate average and standard deviation. To avoid dehydration a moist chamber was used. Wire cutting tests were performed on both porcine brain tissue and CH samples at the wire cutting speed of 5mm/s and a steel wire of diameter 0.16 mm was used. For the brain samples the cerebellum was removed and the two hemispheres were separated. Each hemisphere was positioned in the sample container with the frontal lobe facing upwards. The specimen would slowly shift under gravity and approximately occupy a square prism of length 30 mm, width 30 mm and height 50 mm. CH specimens of the same dimensions were prepared. The schematic of the tests is reported in the results section. The Biomomentum Mach-1™ mechanical testing system was used with a 1.5 N single-axis load cell since the cutting load was small. Ten specimens were tested for both brain tissue and CH.

The tests were performed in a conditioned room at 19°C temperature.

Differential Scanning Calorimetry

Thermograms of the CH and of the two pure components were obtained with the Q 2000 DSC (TA Instruments, USA). Samples were vacuum-dried for 36 h before testing. Specimens had a mass of about 10 mg and the temperature range studied was -40 to 250 °C. The heating/cooling rate was set to 10 °C/min.

Scanning Electron Microscopy

Composite hydrogels blends at different concentrations and their individual components were imaged by SEM using an S-3400N (Hitachi, Japan) in variable pressure mode (100 Pa). Specimens were freeze-fractured and gold-coated using the Auto Sputter Coater (Agar, UK) before the scans began. An accelerating voltage of 15 kV and a working distance of 15 cm were set for the scans of the fracture surface.

Life-sized phantom

The CH can be cast in the shape and size of a human brain and used together with a plastic mock-up skull, to produce a dynamic brain-skull phantom (DBSP). A publicly available MRI dataset, the 01017 MIDAS/NAMIC dataset (http://insight-journal.org/midas/collection/view/190) that depicts the brain of a healthy subject, was used for the development of the life-sized phantom. The scan (256x256x256 voxels, 1mm spacing) was acquired by using a 3T GE scanner. The brain phantom was prepared one day before the scanning session and left at rest in water overnight. Afterwards it was placed and sealed into the skull (filled up with water) approximately 3 hours before the beginning of the scanning session. Briefly, after an accurate segmentation process with 3D Slicer [42], 3D models of the skull and the brain were created. Since only the rigid skull and the deformable brain can be replicated in the setup, a choice has been made to define which anatomical structures to consider and how. The membranes where considered as part of the skull and the ventricles were not included in the model due to the complexity in generating a suitable and reliable hollow structure inside the CH.

A reference prismatic volume was added to the 3D model of the brain in order to simulate the presence of the cerebellum; this enables us to use such feature for the registration step and to reproduce the support function that the spinal cord and the cerebellum have in a real scenario. This block of material is placed in the corresponding space designed in the skull, hence anchoring the brain tissue mimic and preventing it from floating freely in the CSF.

The brain and skull models were rapid prototyped using an Ultimaker 2 3D printer (Ultimaker BV, Geldermalsen, Netherlands) with a layer resolution of 0.2 mm. The material used is Acrylonitrile Butadiene Styrene (ABS, Ultimaker BV, Geldermalsen, Netherlands) that is easy to work and glue. The skull was designed as two halves to facilitate the placement of the phantom. The sealing was assured by removable glue. A craniotomy (5 cm diameter) was performed in correspondence of the left frontal lobe (size and position suggested by a neurosurgeon) for image tracking purposes. The falx cerebri was 3D printed as part of the skull. The falx consists of a thin layer of ABS that divides the two cerebral hemispheres in the brain phantom.

The printed brain was used to create a reusable silicone mould (CS2 silicone rubber, Easy Composites Ltd, Stoke-on-Trent, UK) to cast the brain phantom. The mould was manufactured in two halves to facilitate the extraction of the phantom after the freezing process. Furthermore, the silicone was also selected for being able to deal with the expansion of the water without breaking during the cryogenic process. This allowed us to cast different phantoms with the same mould. Figure 1 shows schematically the complete development of the DBSP.

A support for the DBSP that precisely holds the skull in a position with a -30 degrees tilt in the coronal plane (with respect to the vertical direction) was also 3D printed. The support was designed by boolean subtraction of the skull volume from a cubic shape: this allows the accurate and repeatable positioning of the skull on the holder. The aim was to achieve a good repeatability in the positioning of the skull inside the MRI. In addition the use of the base permits to position the skull while keeping the draining pipe (used for deliquoration and attached to a syringe pump) attached to the apparatus. The black markers visible on the brain phantom in Figure 1 are superficial features used only for image tracking purposes.

Water can be placed inside the skull as a surrogate of the CSF and drained in a controlled way, to simulate deliquoration and the resulting loss of buoyancy, which is recognised as the main cause

of brain shift [19, 20]. The production of CSF can also be mimicked by inverting the flow of water through the syringe pump, injecting liquid inside the skull at a controlled rate through the draining pipe positioned at the bottom of the apparatus.

To have quantitative information about the deformation of the phantom we took several scans of the complete phantom apparatus at two different levels of deliquoration: 100% of the fluid, meaning that the brain shift has not started, and 40% of the fluid left in the skull, which can be considered a plausible worst case scenario in actual surgeries. We segmented the MRI scans and built a 3D finite element (FE) model of the brain phantom using a poro-hyper-viscoelastic constitutive law. The FE simulations of brain shift for different CSF levels, the details of which are provided in a separate contribution (A.E.F., S.G., D.D., "Models and tissue mimics for brain shift simulations", manuscript in preparation), follows precisely the deformation pattern of the phantom (average magnitude error of 0.37 mm). The mesh has 94211 elements and about 36 nodes per cm^2 on the surface, assuring a detailed reproduction of the phantom cerebral cortex geometric features (sulci and gyri). The accurate matching obtained between the FE simulations and the MRI images enabled us to track the deformation of 376 superficial nodes in the area where the maximum deformation of the phantom was recorded (in the region close to the craniotomy) using the results of the numerical calculations. Additional measurements at different CSF levels were collected using a stereocamera set up as described in [43]).
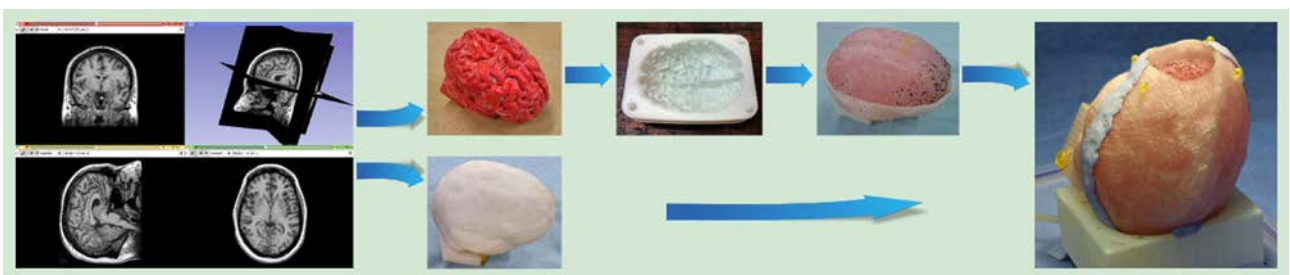

Figure 1 – Development of the DBSP: the mock-up skull and the positive model of the brain were prototyped from the segmentation of the 01017 dataset. A two halves silicone mould was created from the positive brain model and used to cast the CH phantom. The phantom was placed inside the mock-up skull together with the fluid and positioned on the holder.

Results

We evaluated the CH using three different testing protocols: (i) compression tests at large strains, (ii) cyclic indentation-relaxation tests, and (iii) rheometric sweep frequency analysis. We compared the results obtained using the synthetic compound with brain tissue data from the literature. We also tuned the material to reproduce the cutting behaviour of porcine brain tissue and investigated its structure and chemical bonding using scanning electron microscopy and differential scanning calorimetry. Finally, we compared the deformation of a life-sized phantom subjected to brain shift with patient data from the literature.

Mechanical testing

We analyse the mechanical response to compression of (i) synthetic materials, and (ii) the composite hydrogel, at large strains (0.3 true strain). The results are compared with *in vitro* data from the available literature on brain tissue [17]. The results for unconfined compression tests are shown in Figure 2. We divided the measured force by the initial area of the specimen (measured for each test) to calculate compression stress values at 0.3 true strain. Average values and standard deviations are plotted for several synthetic materials, brain tissue experimental data from Miller et al. [17] and the newly designed CH. We used two displacement rates to investigate rate dependent properties of the surrogates (8.3×10^{-2} mm/s and 8.3×10^{-4} mm/s, corresponding to 0.64×10^{-2} s^{-1} and 0.64×10^{-4} s^{-1} strain rate respectively). Additional tests were conducted on all the synthetic materials (only key results are reported for brevity); a comprehensive qualitative overview of the mechanical characteristics of all synthetic materials tested is provided in Table 1, with the first two columns summarising the results shown in Figure 2. Matching the compression stress at large deformation is a mandatory characteristic for reproducing the dynamic mechanical behaviour of the tissue as a whole. For this reason, none of the synthetic materials investigated represents a reliable substitute for brain tissue phantoms, except for the CH. Hence, the following tests focus on the CH only, confirming that it is a good surrogate candidate for the brain tissue.
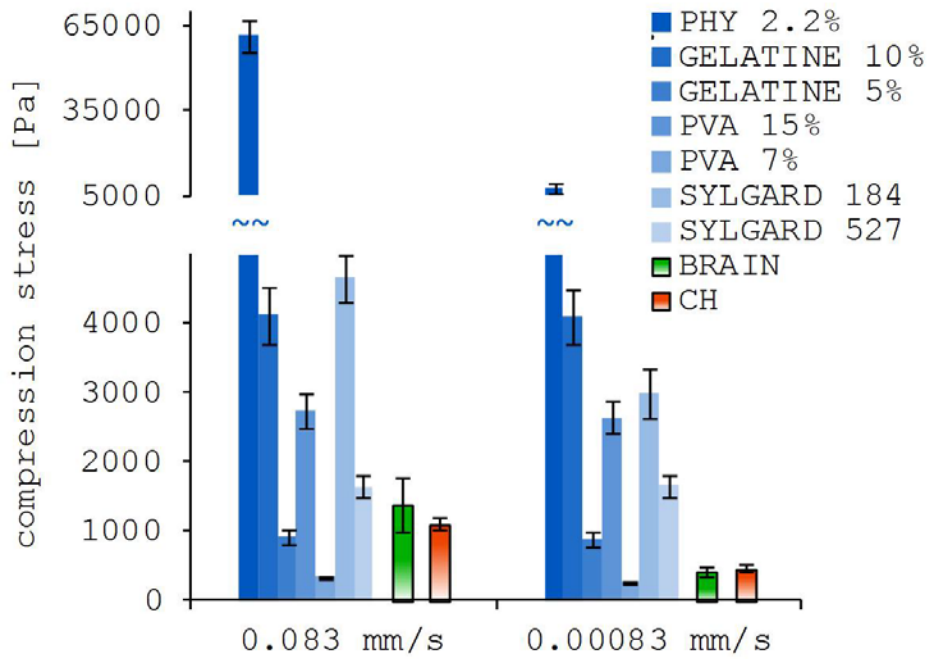
Figure 2- Average and standard deviation of compressive stress at 0.3 true strain. Results are reported for several synthetic materials tested by the authors and brain tissue measurement from the literature for two different displacement rates.

		CSM	CSS	RD	HE	TS	TRD
PHY	2.2%			✓	✓	✓	
GELATINE	10%					✓	
	5%	✓					
PVA	15%					✓	
	7%		✓				
SYLGARD 184				✓	✓		
SYLGARD 527		✓			✓		
CH	6% PVA 0.85% PHY	✓	✓	✓	✓	✓	✓

The non-   linear

Table 1- Qualitative summary of synthetic materials capabilities. CSM: compressive stress similar to brain at 8.3 x 10^{-2} mm/s displacement rate. CSS: compressive stress similar to brain at 8.3 x 10^{-4} mm/s displacement rate. RD: rate dependency; HE: hyperelastic behaviour; TS: tunable stiffness; TRD: tunable rate dependent characteristics.

hyperelastic responses of the CH (average and standard deviation) at medium and low

displacement rates, 8.3 x 10^{-2} mm/s and 8.3 x 10^{-4} mm/s respectively, are shown in Figure 3a and

Figure 3b. A comparison of the averaged experimental values obtained for brain tissue from the

literature [17] is also provided. The lowest loading speed available on our equipment is 8.3 x 10^{-4}

mm/s, which is sufficiently low for viscoelastic, poroelastic and rate dependent effects to be

negligible, as verified by FE modelling of the compression test, the results of which are not

reported here for brevity. This speed is therefore deemed to be within the low-displacement-rate

regime, and our results are comparable with the brain measurements available in the literature that were conducted at slightly lower speeds (8.3×10^{-5} mm/s).

The CH mechanical response to indentation-relaxation tests (average and standard deviation) performed at performed at 3 mm/s and 1 mm/s indentation speed (approximately 0.066 s^{-1} and 0.022 s^{-1} strain rates respectively, defined as the instantaneous displacement rate of the indenter divided by the instantaneous displacement [40]) is shown in Figure 3c and Figure 3d respectively. *In vivo* indentation tests on porcine brain from Gefen et al. [37] are reported for comparison. In the first indentation cycle at 3 mm/s, the peaks show values of 14 gf and 15.3 gf for the CH and the brain respectively.

CH storage (G') and loss (G") shear moduli (average and standard deviation) measured over a large frequency range (0.01 to 25 Hz, corresponding to the shear rates of $0.64 \times 10^{-3} - 1.6$ s^{-1}) are shown in Figure 3e and Figure 3f respectively. Brain tissue *in vitro* measurements available in the literature [41] are reported for comparative purposes. The results show that the CH storage and loss moduli are in agreement with the majority of brain tissue data reported in other studies.

Wire cutting tests were performed on both porcine brain tissue and CH samples at the wire cutting speed of 5mm/s and a steel wire of diameter 0.16 mm was used, according to testing protocols conventionally used to assess the resistance of materials to tearing and cutting [44, 45]. The schematic of the tests is shown in Figure 4a. The best mimicking of the cutting response of brain tissue was achieved lowering the concentration of PVA since this component tends to create a strong elastic and stretchable network that increases the cutting resistance of the composite hydrogel. We achieved the best match by mixing PVA 2.25% and PHY 0.85% separate solutions in 1:1 weight ratio (Figure 4b).
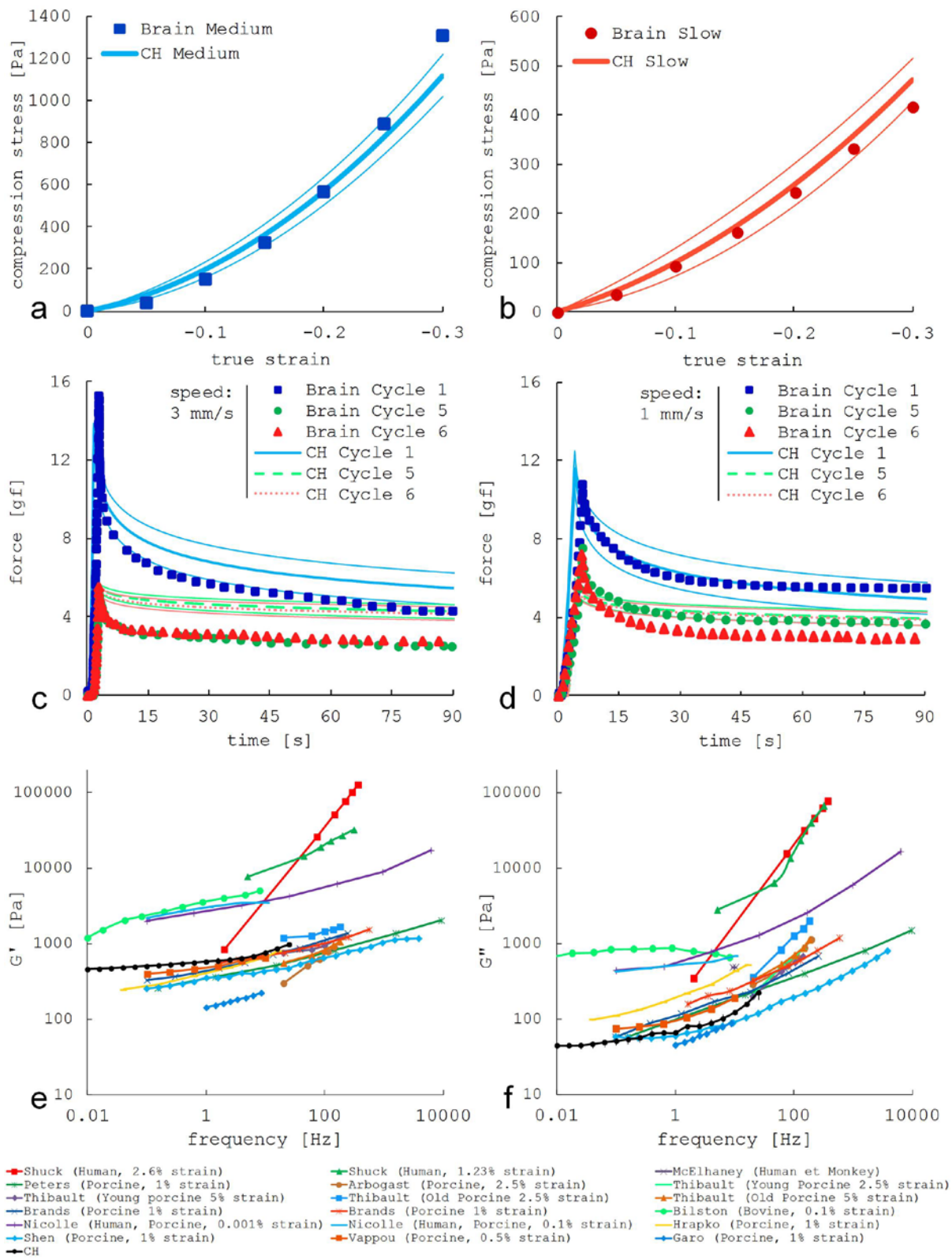
Figure 3- Mechanical testing results on CH and comparison with brain measurements available in the literature. Unconfined compression test at a) 8.3 x 10^{-2} mm/s and b) 8.3 x 10^{-4} mm/s; cyclic indentation-relaxation tests at c) 3 mm/s and d) 1 mm/s; e) storage and f) loss moduli measured by sweep frequency analysis.
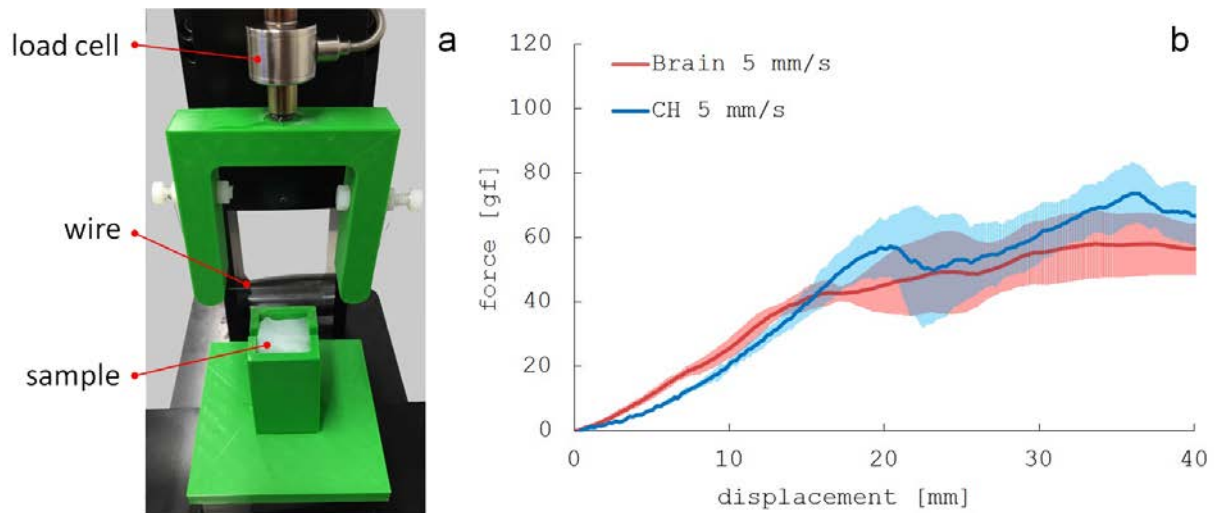
Figure 4- a) Wire cutting testing set up; b) Cutting forces averages and standard deviations for porcine brain tissue and CH (2.25% PVA, 0.85% PHY) at 5 mm/s cutting speed and 0.16 mm wire diameter.

Scanning Electron Microscopy

To reveal the changes in the porous structure we performed scanning electron microscope scans of the new hydrogel and the pure components. Figure 5a (from *1* to *6*) shows that both PVA and PHY are able to reach gelation and create networks. The picture also shows how increasing the polymer concentrations resulted in smaller pores for the three different materials (Figure 5 a, from *1* to *3*, *4* to *6*, *7* to *9* respectively), where the scale bar is given as reference. Furthermore, a denser network is noticeable, with polymer fibres that branch more frequently, causing the increase in stiffness measured during the mechanical tests. The brain-tuned concentration for the novel hydrogel is depicted in Figure 5a-8 (PVA 6% + PHY 0.85%). It is worth noticing how the CH network substantially changes from the pure components examining the groups of images vertically in Figure 5a. It is clear that the solid branches assume a new morphology.
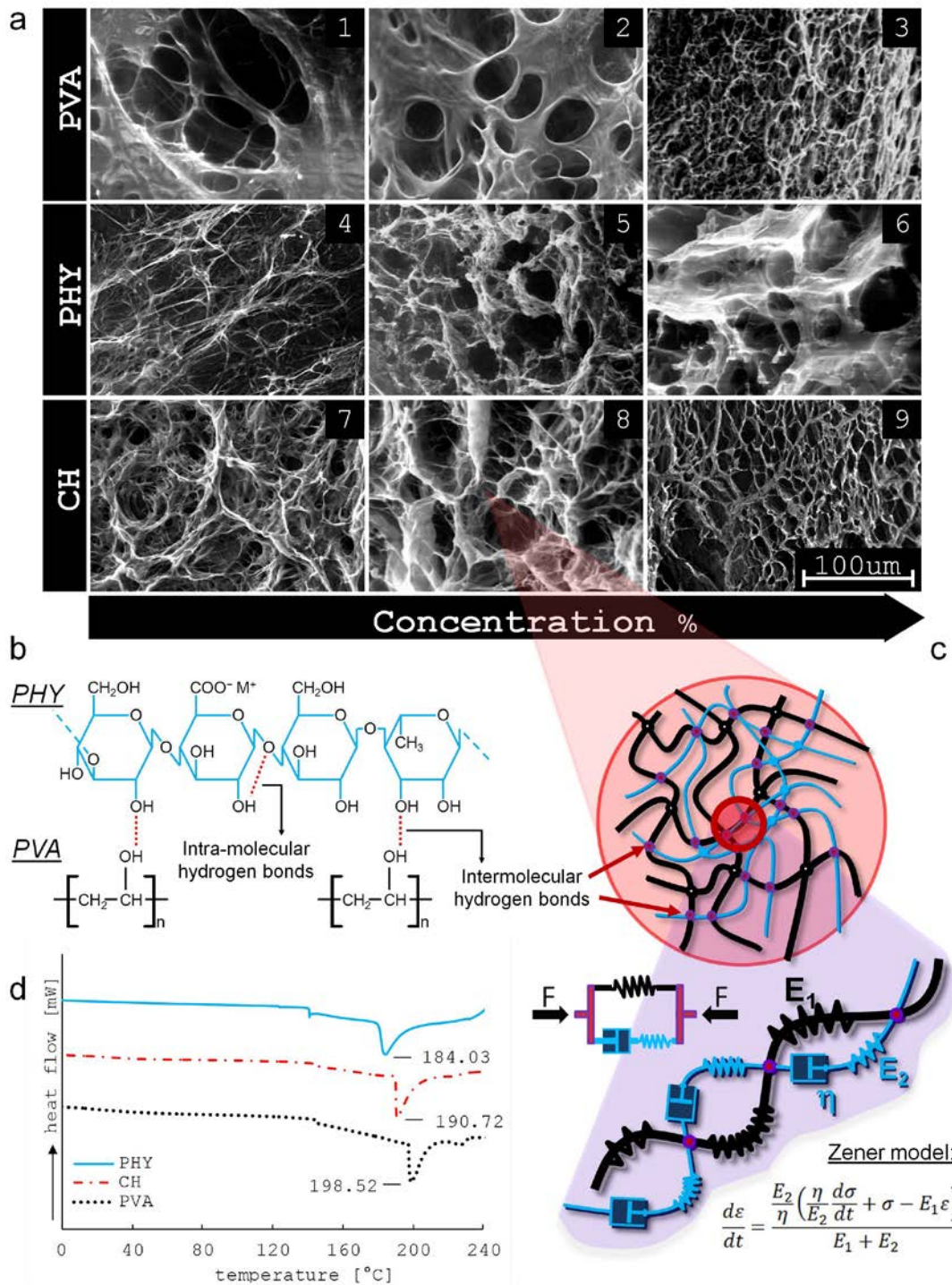
Figure 5- a) SEM images for PVA, PHY and CH at increasing concentration values. In particular: 1) PVA 4%; 2) PVA 6%; 3) PVA 8%; 4) PHY 0.56%; 5) PHY 0.85%; 6) PHY 1.13%; 7) CH = PVA 4% + PHY 0.56%; 8) CH = PVA 6% + PHY 0.85%; 9) CH = PVA 8% + PHY 1.13%; b) Intra-molecular and Intermolecular hydrogel bonds; c) Coupled network model in analogy with the Zener model from the viscoelasticity theory; d) DSC thermographs for pure PHY, CH and pure PVA.

Differential Scanning Calorimetry

We performed thermal analysis using DSC to study the interaction of the two polymers by

monitoring the shift in the melting temperature values (T_m) of the composite material and its

individual constituents (Figure 5d). In case of immiscible components two distinct peaks have been

noticed [46, 47]. The melting temperature of PHY was measured to be 184.03 °C, the CH showed

a peak of 190.72 °C while pure PVA had a melting temperature of 198.52 °C (Figure 5d).

Life-sized phantom

To further validate that the CH provides an accurate replication of the mechanical response of

brain tissue, we designed and developed a life-sized human phantom. The aim was to

demonstrate that a CH phantom can replicate the complex deformation of the human brain during

brain shift in a configuration that closely replicates surgical procedures involving craniotomies.

Since the mechanical characterisation has been conducted mainly on small-size specimens we

show that the CH correctly mimics the brain tissue deformations on a larger scale. In addition, this

set up involves complex boundary conditions such as the brain-skull interaction.

Figure 6c shows two views of the phantom in the MRIs (3D Slicer [42], http://www.slicer.org) and a

reconstruction (particular of the left frontal lobe) of the undeformed and deformed phantom

surfaces (Figure 6d, Paraview [48]). Although the averaged surface displacements were computed

at every node, only a few representative nodes were selected to be displayed in Figure 6d: here,

the white dots represent the position of the selected nodes of the mesh in the undeformed

phantom, while the green dots show the position of the same nodes after the shift. A vector field

representing the displacement is overimposed to the volumetric data in Paraview. The average

displacement observed is 8.17 mm and has been compared with human brain shift data, obtained

from patients undergoing similar surgical procedure, from the literature [19, 49-51] (Figure 6e).

Experiments have been conducted to assess the rehydration properties of the CH and have shown

the ability to maintain structural integrity in shift-like deformations (results not reported for brevity).

Tests also showed that life-sized phantoms are able to recover their initial shape once the skull has

been refilled with fluid. Furthermore, the life-sized phantom overall deformation is not only due to

the changes in buoyancy caused by draining the water drainage but also to a combination of

mechanisms at different scales, enabled by the viscoelasticity and porosity characteristic of the

solid matrix of the CH. This has been observed by quickly removing the water from the skull (in

about 100s) and tracking the surface deformation over time (using a stereocamera set up [43]).

The shift in absence of water was about 13% of the total deformation after the water was removed and had not reached the steady state after 20 minutes.
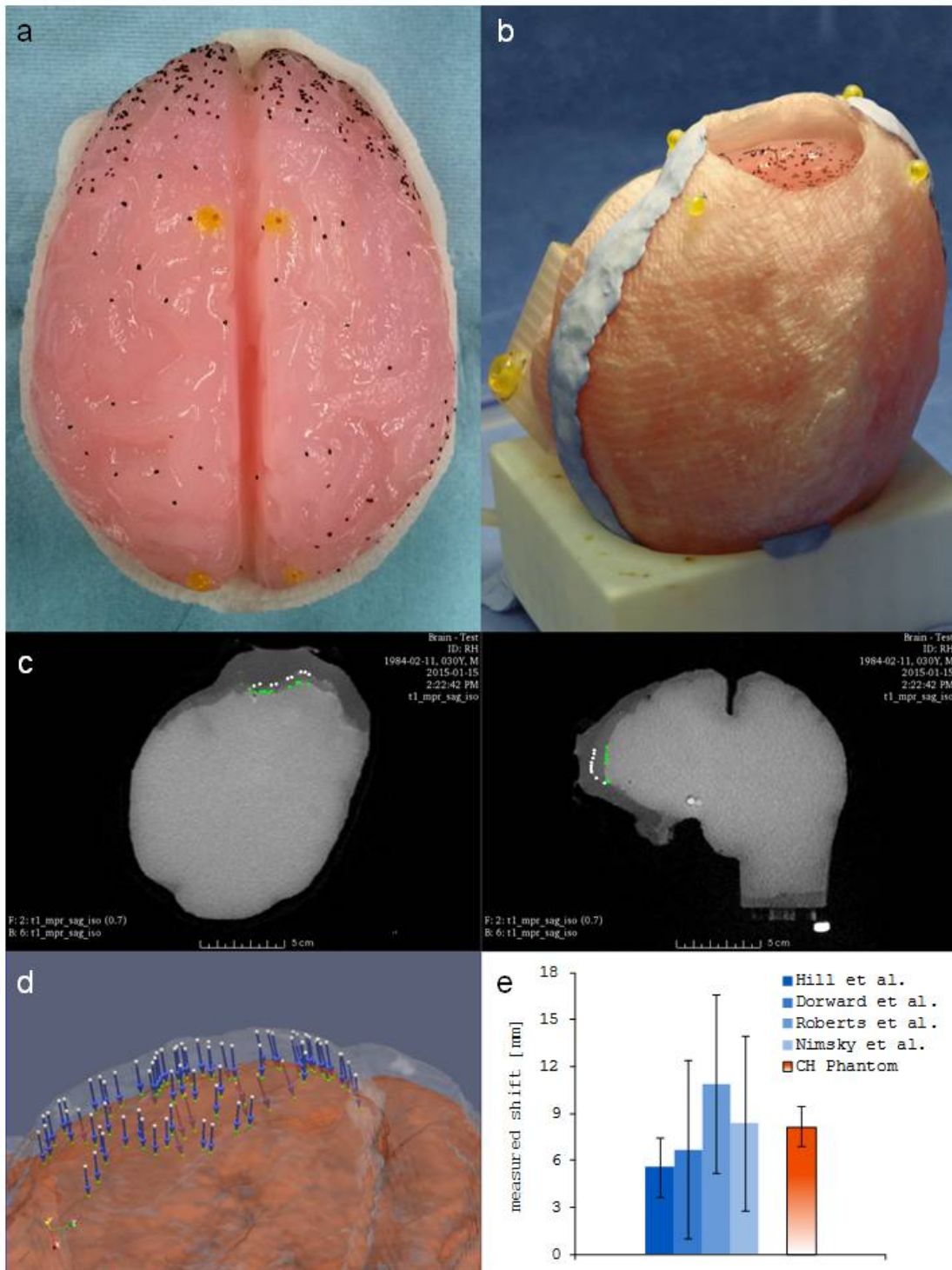

Figure 6 – a) Life-sized phantom of the human brain; b) Experimental apparatus for the brain shift study. The craniotomy in the 3D printed water-proof skull has been performed according to the specifics of the surgeon but is not considered in this test. c) MRI scans of the apparatus; d) 3D reconstructions of volumes and deformations: the white dots represent features in the undeformed phantom (100% of fluid); green dots are the same features in the deformed (40% of fluid) phantom; the blue arrows represent the deformation fields of the considered features; e) Average value of the deformation field measured in the phantom compared with data from the literature.

Discussion

The combined mechanical/analytical testing strategy presented above has been used to demonstrate that it is possible to develop and fabricate an inexpensive and easy-to-make synthetic surrogate that reproduces the dynamic mechanical response of brain tissue. Here we discuss the results presented in the previous section and conclude that the mechanical properties of the novel CH are in excellent agreement with the brain tissue mechanical response, as demonstrated by the means of three different testing protocols.

Adopting a standard unconfined compression protocol, the investigation focused on testing readily available polymers (PHY, Gelatine, PVA, Sylgard 184 and 527) along with the new CH for large deformations (0.3 true strain, Figure 2). We used two different displacement rates to highlight the rate dependent properties of each synthetic material. This allowed us to assess the feasibility of using individual commercially available components for mimicking the complex mechanical response of brain tissue. Polymers, such as Gelatine and PVA, can be tuned by varying the solute concentration in order to obtain either a more compliant or a stiffer response. Figure 2 shows that Gelatine gels exhibit an averaged compression stress of 4116.25 Pa at 10% concentration and 931.56 Pa at 5% concentration, while PVA goes from 2734.78 Pa to 340.47 Pa when halving the concentration (15% to 7%). The key result here is that these polymers do not show rate dependent properties [45], exhibiting constant stiffness when loaded with different displacement rates. This is due to their elementary polymer networks, which exhibit a simple elastic behaviour.

PHY showed excellent rate-dependent properties (peak compression stress of 61500 Pa and 8148.10 Pa for 8.3×10^{-2} mm/s and 8.3×10^{-4} mm/s displacement rate respectively) and stiffness-tunability (by varying the powder concentration in the aqueous solution), along with a pronounced hyperelastic response in compression. However, the results showed in Figure 2 for 2.2% PHY concentration highlight the high strength of the compound; this is not in line with the soft tissue characteristics we were seeking to mimic (brain tissue compression stress from the literature: 1380.53 Pa and 423.48 Pa for the medium and slow strain rate respectively). Furthermore, PHY becomes increasingly brittle as the polymer concentration is lowered, hence

making its applicability as a brain phantom surrogate unlikely if used in isolation as a pure compound.

Sylgard 184 exhibited good rate-dependent properties and a non-linear elastic response when tested in compression. However, the gel is too stiff and the lack of stiffness-tunability rules out the usability of this gel as a surrogate for brain tissue phantoms.

Although Sylgard 527 is presented in the literature as a good substitute material for the brain tissue, its mechanical response is lacking in the rate-dependent characteristics (Figure 2). It is shown that the gel exhibits averaged compression stress of 1648.59 Pa and 1658.34 Pa for 8.3 x 10^{-2} mm/s and 8.3 x 10^{-4} mm/s displacement rate respectively. The compression tests, that were carried out by varying the displacement rate over two orders of magnitude, prove that this gel can only be suitable for applications involving displacement rates of approximately 8.3 x 10^{-2} mm/s.

The new CH has been designed by balancing the mutual concentration of two compounds: PVA and PHY. We achieved the best match in compression, indentation and shear by mixing PVA 6% and PHY 0.85% separate solutions in 1:1 weight ratio and for cutting by mixing PVA 2.25% and PHY 0.85% separate solutions in 1:1 weight ratio. The PVA is responsible for creating the solid network by means of a freezing step. The PHY is kept at low concentrations to prevent an excessive increase in stiffness, while providing good rate-dependent properties to the mixture. The response of the CH is in very good agreement with brain compression tests from the literature. Figure 2 shows a compression stress of 1116.38 ± 100.37 Pa for the CH and 1380.53 ± 393.13 Pa for brain tissue when compressed at 8.3 x 10^{-2} mm/s. Furthermore, the stiffness of the material changes if loaded at 8.3 x 10^{-4} mm/s, exhibiting a compression stress of 472.59 ± 43.8 Pa, in comparison with a value of 423.48 ± 79.91 Pa obtained for the brain tissue. The complete unconfined compression curves are reported in Figure 3a and Figure 3b: the hyperelastic characteristic of the CH, when subjected to large deformations and tested over a range of velocities spanning over two orders of magnitude, is shown to be in agreement with the brain mechanical response (experimental results reported on brain tissue lie in the standard deviation range of our measurements). This is further supported by both cyclic indentation-relaxation and sweep frequency shear tests. The excellent agreement between the force response of the CH and the *in-vivo* measurements carried out by Gefen et al. [37] (Figure 3c and Figure 3d) for indentation

rates of 1 and 3 mm/s demonstrates how the CH is able to accurately reproduce complex dynamic

mechanical responses that involve both compressive and tensile stress (i.e. indentation). The

relaxation behaviour of the brain tissue during Cycle 1 (first unconditioned indentation test) lies well

inside the standard deviation range of the CH (Figure 3c and Figure 3d), especially for the velocity

of 1 mm/s. Furthermore, the significant mechanical hysteresis and consequent not-recoverable

deformation (peak values considerably drop from Cycle 1 to Cycle 5 and 6) that CH exhibits under

cyclic loading (Figure 3c and Figure 3d) is similar to the hysteretic behaviour obtained for brain

samples and improves the fidelity of the material to applications that involve repetitive loading

cycles.

The rheometric test results prove the suitability of CH for reproducing the correct mechanical

response of brain tissue in shear over a large frequency range (0.01 – 25 Hz, corresponding to the

shear rates of $0.64 \times 10^{-3} – 1.6 \ s^{-1}$). Measurements obtained for storage and loss moduli are

included and compared with brain tissue measurements reproduced from the biorheological

literature (Figure 3e and Figure 3f).

Although we showed that the CH is able to mimic to mechanical behaviour of brain tissue for slow

and medium rates (from 0.00083 mm/s to 0.083 mm/s), these might seem relatively low if

compared to the rate of certain real-life applications (e.g., touch, device implantation, etc.).

However, testing at medium indentation rates (1 mm/s and 3 mm/s) has been successfully carried

out (Result section, Figure 3c and d). Reproducing fast rate responses is indeed feasible, but

requires retuning of the concentrations of the compounds and their mixing ratio.

Since the PVA tends to create a strong elastic and stretchable network that increases the cutting

resistance of the composite hydrogel, a better mimicking of the cutting response of brain tissue

was achieved lowering the concentration of PVA. Although this new mixture is satisfactory for

reproducing the mechanical response of brain tissue under cutting, lowering the PVA concentration

leads to a slight decrease in stiffness, which is noticeable in the indentation part of the curve in

Figure 4b. Therefore currently one should choose the CH concentration according to the desired

application. It is also envisaged that a functionally graded CH can be produced by varying the

concentration of PVA through the thickness of the brain phantom to simultaneously mimic cutting

and brain shift. This will constitute part of our future investigations. We are also confident that the

mechanical behaviour of the CH under submerged conditions is similar to that of the brain in a similar setup. In fact, we have shown that the overall response of the two materials in saturated conditions (compression and indentation tests) is in good agreement. Additionally, their solid matrices also exhibit similar mechanical properties (demonstrated through rheological tests). Since water and CSF are comparable in terms of viscosity and density, the frictional interaction between the solid and the fluid phases in the two materials are bound to be similar. Consequently, CH and brain are to be expected to show equivalent behaviour when submerged. This is further confirmed by looking at the pore size of the CH in the SEM scans (Figure 5a-8) which is very close to the pore size previously observed for brain tissue [52]. Also, the brain and the CH have similar mass density (close to that of water [20]). Moreover, moist conditions and in particular moist chambers were used when characterizing brain tissue in several studies [53-57]. This further proves the validity of our testing protocol. It is worth noting that the above is true only for the range of displacement rates analysed when using the CH composition reported in this study. Also, although we foresee to widen the applicability of the composite hydrogel to *in-vivo* applications and use at body temperature, further mechanical analyses are needed to investigate the changes in the CH mechanical properties with temperature and explore its suitability (and tunability) for applications in different environmental conditions, potentially in the presence of live cells.

Focusing on binary polymer networks, Brownsey & Morris [34] distinguished between two types of binary gels: type I gels, where one polymer forms a network and the second is entrapped in the first one and type II, where both the polymers are able to create a network. Type II gels are further distinguished in three different networks: coupled, interpenetrating, phase separated networks. Coupled networks are characterized by chemical interactions between the two polymer networks. A coupled network can also form if molecular bindings are present. Interpenetrating networks are formed by two distinct polymer structures that span the entire system. No chemical bindings are present, only topological interactions (i.e. entanglement). In phase separated networks usually one polymer form the dominant phase (continuous network) and the other the included phase (filler network) with absence of chemical interaction.

We now direct our attention to the DSC measurements, where the presence of a single T_m peak in the thermograph of CH (Figure 5d) does not necessarily show that a new, single material has

formed, but that the two components are at least miscible (in case of immiscible components two distinct peaks have been noticed [46, 47]). However, this excludes both the interpenetrating and phase separated network models. Type I binary network can be excluded because there are conditions to favour gelation of both the components in the blend (Figure 5a). Furthermore, previous Fourier Transform Infrared analysis (FTIR) on PVA-Polysaccharide blends (Chitosan in particular) [58] report changes of the band shape and a shift towards lower frequencies of the top of the band in the OH stretching region. This indicates the presence of strong hydrogen bonding interactions between OH of PVA and OH of the polysaccharide in the blend, since hydrogen bonding usually causes the stretching vibration to shift to a lower frequency. In another study, Alhosseini et al. [10] link the improved mechanical properties (in terms of strength) of PVA-Chitosan blends to the interaction between the two polymeric networks through (i) hydrophobic side-chain aggregation and (ii) hydrogen bonds between OH groups in the polymeric macromolecules. In order to verify that this is the case for our composite hydrogel constructs, we carried out additional compression tests (not reported in this work for brevity) on the CH blend (PVA 6% - PHY 0.85%) and the separate components (PVA 6% and PHY 0.85%). The results show that the blend strength is considerably higher than the sum of the strengths of the two single components: the CH compression stress was approximately 27 times higher than pure PVA and 40 times higher than pure PHY, proving that an interaction between the two polymer networks exists. Moreover, being a tetrasaccharide, the PHY has a molecular structure characterised by available OH groups at the free ends of the aromatic hydrocarbon (Figure 5b). For this reason we believe that the CH presents a type II coupled network structure (Figure 5c) where the interaction between the two polymer networks is not due to chemical cross-links but rather to hydrogen bonds between the OH groups of PVA and PHY (Figure 5b).

Therefore, it appears that the physical interaction between the two components is responsible for the creation of a new network structure that improves the mechanical characteristics of the CH, compared with those of any other synthetic material used so far as a brain tissue surrogate. In particular, the novel hydrogel shows tuneable stiffness and highly stretchable properties that are mainly related to the elastic behaviour of the PVA network (represented here by the Young's modulus E_1 in Figure 5c), as well as tuneable viscoelastic properties and non-linear elastic

24

characteristics that are controlled by the PHY network (represented here by the Young's modulus E_2 and the viscosity coefficient η in Figure 5c). The overall mechanical response can be approximated, even though only qualitatively in the present work, to a Zener model from the viscoelasticity theory (Figure 5c). Additional testing is required in order to confirm this.

An important advantage of our novel material is the option to tune its mechanical response by varying the relative concentrations of PVA and PHY. In particular, the strong adaptability of CH allows the design of highly viscous as well as strongly elastic mixtures. Thus, if a surrogate with different properties is needed (e.g. liver, skin, kidney, cartilage etc.), the development of a suitable phantom made of PVA + PHY will still be possible. The authors would like to point out once again that the novel material has been design and tuned for mimicking the mechanical response of brain tissue over a wide range of strain rates and testing conditions. Although the structure of the synthetic construct has been shown to have similar pores size when compared to the extracellular matrix of brain according to the literature, the matching does not extend to the exact reconstruction of the complex organic micro-structures and chemical characteristic of the brain tissue (which might be desirable in order to extend the range of applications of the CH), which has not yet been fully achieved for the composite hydrogel described in the present work.

In this work we also presented and described the design of a life-sized human brain phantom obtained from a patient-specific MRI dataset. Although the life-sized phantom reproduces some superficial details (sulci and gyri that can be useful for localization purposes), the principal blood vessels and nerves are not present in this preliminary model. A potential solution that we aim to explore in future studies is the use of the CH at higher concentrations (as to control the stiffness of the resulting structures). This can be casted in complex shapes and coloured with different dies in order to reproduce the principal vessels and nerves. The pre-prepared structures then can be placed in the mould before casting the final CH and embedded into the bulk of the life-sized phantom.

At this preliminary stage, the phantom is also missing the ventricular apparatus, the tentorium and the meninges. Consequently, in the current state of development, the number of surgical procedures that can be performed using the synthetic phantom is limited to tumour resection surgery, surgical exploratory techniques, and some implantation procedures. This is currently

being addressed by the addition of several other anatomical features within the phantom, which will be presented in a separate contribution. Measurements of the deformation field produced by the loss of CSF have been carried out using MRI scans. This technique allowed us to have a controlled environment and to accurately reproduce the brain shift phenomenon in a laboratory setting. The average amount of shift has been compared with measurements from the literature [19, 49-51] confirming a very good agreement (see Figure 6). The shift value measured in the left frontal lobe of the phantom (8.17 mm) lies well inside the standard deviation range of the measurements reported by three different studies [19, 50, 51].

Conclusions

All the results hereby presented prove the superior capabilities of the newly developed composite hydrogel as surrogate material for brain tissue phantoms. The novel hydrogel presented here is suitable for reproducing complex deformation scenarios such as brain shift, surgical indentation and palpation. It mimics the organic tissue's mechanical behaviour in compression, indentation, relaxation, hysteresis and shear.

We recognise the importance of reproducing tearing, cutting and dissociation of organic tissues. We demonstrated that varying the concentration of PVA from 6% to 2.25% the CH is able to reproduce the mechanical response of the brain tissue to cutting. The use of the new material is envisaged for surgery planning, preoperative tests, robot motion compensation tests, surgical training or any other applications where the dynamic response is crucial.

We believe that the life-sized phantom has the potential to provide a fine tool for the investigation of traumatic brain injury (TBI) studies. However, a higher grade of neuroanatomical similarity is needed. Once anatomically improved, the life-sized phantom could be tested to perform realistic measurements for the validation and advancement of computational modelling of traumatic brain injury, a field that nowadays is undergoing great development.

It is worth noting that the current CH formulation will mimic the mechanical behaviour of brain tissue for surgical rates only (slow and medium rates). Further investigations are needed to adapt the CH to match the brain response at higher rates, which are typical of impact loading.

Furthermore, given the biocompatibility of its constituents, the hydrogel is likely to be biocompatible. Therefore we foresee investigating the possibility of introducing CH as a porous soft medium for cell cultures, as well as a study of the effects of mechanical tailored scaffolds on cell growth, migration and differentiation. Alterations in mechanical properties caused by the introduction of cells into the material might be overcome by tuning concentrations of the two components. However, this aspect has not been yet investigated and at present it represents a limitation of this study to be overcome by performing specialised studies focused on cell seeding and its effect on the mechanical behaviour of the CH.

Acknowledgements

Author contributions

A.E.F., F.R. y B. and D.D. conceived the theoretical approach. A.E.F. and F.M. designed and tested the material. A.E.F. developed and tested the material to its final stage. A.E.F. and S.G. designed and manufactured the life-sized phantom and analysed data. A.E.F., S.G. and D.D. wrote the manuscript.

Competing financial interests

All of the authors, employed by academic institutions, have no conflicts of interest to declare.

References

1. Chikwe, J., A.C. de Souza, and J.R. Pepper, *No time to train the surgeons.* BMJ, 2004. **328**(7437): p. 418-9.
2. Akhtar, K.S., A. Chen, N.J. Standfield, and C.M. Gupte, *The role of simulation in developing surgical skills.* Curr Rev Musculoskelet Med, 2014. **7**(2): p. 155-60.

3.   Holland, J.P., L. Waugh, A. Horgan, V. Paleri, and D.J. Deehan, *Cadaveric hands-on training for surgical specialties: is this back to the future for surgical skills development?* J Surg Educ, 2011. **68**(2): p. 110-6.

4.   Leong, J.J., D.R. Leff, A. Das, R. Aggarwal, P. Reilly, H.D. Atkinson, R.J. Emery, and A.W. Darzi, *Validation of orthopaedic bench models for trauma surgery.* J Bone Joint Surg Br, 2008. **90**(7): p. 958-65.

5.   Michelson, J.D., *Simulation in orthopaedic education: an overview of theory and practice.* J Bone Joint Surg Am, 2006. **88**(6): p. 1405-11.

6.   Strom, P., A. Kjellin, L. Hedman, E. Johnson, T. Wredmark, and L. Fellander-Tsai, *Validation and learning in the Procedicus KSA virtual reality surgical simulator.* Surg Endosc, 2003. **17**(2): p. 227-31.

7.   Mabrey, J.D., W.D. Cannon, S.D. Gillogly, J.R. Kasser, H.J. Sweeney, B. Zarins, H. Mevis, W.E. Garrett, and R. Poss, *Development of a virtual reality arthroscopic knee simulator.* Stud Health Technol Inform, 2000. **70**: p. 192-4.

8.   Smith, A.M., R.M. Shelton, Y. Perrie, and J.J. Harris, *An initial evaluation of gellan gum as a material for tissue engineering applications.* J Biomater Appl, 2007. **22**(3): p. 241-54.

9.   Norton, A.B., R.D. Hancocks, and L.M. Grover, *Poly (vinyl alcohol) modification of low acyl gellan hydrogels for applications in tissue regeneration.* Food Hydrocolloids, 2014. **42, Part 3**(0): p. 373-377.

10.   Alhosseini, S.N., F. Moztarzadeh, M. Mozafari, S. Asgari, M. Dodel, A. Samadikuchaksaraei, S. Kargozar, and N. Jalali, *Synthesis and characterization of electrospun polyvinyl alcohol nanofibrous scaffolds modified by blending with chitosan for neural tissue engineering.* International Journal of Nanomedicine, 2012. **7**: p. 25-34.

11.   Steele, J., S. McCullen, A. Callanan, H. Autefage, M. Accardi, D. Dini, and M. Stevens, *Combinatorial scaffold morphologies for zonal articular cartilage engineering.* Acta biomaterialia, 2014. **10**(5): p. 2065-2075.

12.   Discher, D.E., D.J. Mooney, and P.W. Zandstra, *Growth Factors, Matrices, and Forces Combine and Control Stem Cells.* Science, 2009. **324**(5935): p. 1673-1677.

13.   Saha, K., A.J. Keung, E.F. Irwin, Y. Li, L. Little, D.V. Schaffer, and K.E. Healy, *Substrate Modulus Directs Neural Stem Cell Behavior.* Biophysical Journal, 2008. **95**(9): p. 4426-4438.

14.   Engler, A.J., C. Carag-Krieger, C.P. Johnson, M. Raab, H.Y. Tang, D.W. Speicher, J.W. Sanger, J.M. Sanger, and D.E. Discher, *Embryonic cardiomyocytes beat best on a matrix with heart-like elasticity: scar-like rigidity inhibits beating.* J Cell Sci, 2008. **121**(Pt 22): p. 3794-802.

15.   Arulmoli, J., M.M. Pathak, L.P. McDonnell, J.L. Nourse, F. Tombola, J.C. Earthman, and L.A. Flanagan, *Static stretch affects neural stem cell differentiation in an extracellular matrix-dependent manner.* Scientific Reports, 2015. **5**: p. 8499.

16.   Franze, K., *The mechanical control of nervous system development.* Development, 2013. **140**(15): p. 3069-77.

17.   Miller, K. and K. Chinzei, *Constitutive modelling of brain tissue: Experiment and theory.* Journal of Biomechanics, 1997. **30**(11–12): p. 1115-1121.

18.   Franceschini, G., D. Bigoni, P. Regitnig, and G.A. Holzapfel, *Brain tissue deforms similarly to filled elastomers and follows consolidation theory.* Journal of the Mechanics and Physics of Solids, 2006. **54**(12): p. 2592-2620.

19.   Roberts, D.W., A. Hartov, F.E. Kennedy, M.I. Miga, and K.D. Paulsen, *Intraoperative brain shift and deformation: a quantitative analysis of cortical displacement in 28 cases.* Neurosurgery, 1998. **43**(4): p. 749-58; discussion 758-60.

20.   Dumpuri, P., R.C. Thompson, B.M. Dawant, A. Cao, and M.I. Miga, *An atlas-based method to compensate for brain shift: Preliminary results.* Medical Image Analysis, 2007. **11**(2): p. 128-145.

21. Hartkens, T., D.L. Hill, A.D. Castellano-Smith, D.J. Hawkes, C.R. Maurer, Jr., A.J. Martin, W.A. Hall, H. Liu, and C.L. Truwit, *Measurement and analysis of brain deformation during neurosurgery.* IEEE Trans Med Imaging, 2003. **22**(1): p. 82-92.

22. Saltzman, W.M. and M.L. Radomsky, *Drugs released from polymers: diffusion and elimination in brain tissue.* Chemical Engineering Science, 1991. **46**(10): p. 2429-2444.

23. Firbank, M. and D.T. Delpy, *A design for a stable and reproducible phantom for use in near infra-red imaging and spectroscopy.* Physics in Medicine and Biology, 1993. **38**(6): p. 847.

24. Kurth, C.D., H. Liu, W.S. Thayer, and B. Chance, *A dynamic phantom brain model for near-infrared spectroscopy.* Phys Med Biol, 1995. **40**(12): p. 2079-92.

25. Cloyd, J., N. Malhotra, L. Weng, W. Chen, R. Mauck, and D. Elliott, *Material properties in unconfined compression of human nucleus pulposus, injectable hyaluronic acid-based hydrogels and tissue engineering scaffolds.* European Spine Journal, 2007. **16**(11): p. 1892-1898.

26. DeLorenzo, C., X. Papademetris, K.P. Vives, D.D. Spencer, and J.S. Duncan. *A realistic brain phantom for 3D deformation recovery.* in *4th IEEE International Symposium on Biomedical Imaging: From Nano to Macro.* 2007. Arlington: IEEE.

27. Brands, D.W., P.H. Bovendeerd, G.W. Peters, J.S. Wismans, M.H. Paas, and J.L. van Bree. *Comparison of the dynamic behavior of brain tissue and two model materials.* in *43rd Stapp Car Crush Conference.* 1999. San Diego, California, USA: SAE.

28. Alexandre, N., J. Ribeiro, A. Gärtner, T. Pereira, I. Amorim, J. Fragoso, A. Lopes, J. Fernandes, E. Costa, A. Santos-Silva, M. Rodrigues, J.D. Santos, A.C. Maurício, and A.L. Luís, *Biocompatibility and hemocompatibility of polyvinyl alcohol hydrogel used for vascular grafting—In vitro and in vivo studies.* Journal of Biomedical Materials Research Part A, 2014. **102**(12): p. 4262-4275.

29. Baker, M.I., S.P. Walsh, Z. Schwartz, and B.D. Boyan, *A review of polyvinyl alcohol and its uses in cartilage and orthopedic applications.* J Biomed Mater Res B Appl Biomater, 2012. **100**(5): p. 1451-7.

30. Silva-Correia, J., B. Zavan, V. Vindigni, T.H. Silva, J.M. Oliveira, G. Abatangelo, and R.L. Reis, *Biocompatibility Evaluation of Ionic-and Photo-Crosslinked Methacrylated Gellan Gum Hydrogels: In Vitro and In Vivo Study.* Advanced healthcare materials, 2013. **2**(4): p. 568-575.

31. Mansur, H.S., E. de S. Costa Jr, A.A.P. Mansur, and E.F. Barbosa-Stancioli, *Cytocompatibility evaluation in cell-culture systems of chemically crosslinked chitosan/PVA hydrogels.* Materials Science and Engineering C, 2009. **29**(5): p. 1574-1583.

32. Shokrgozar, M.A., F. Mottaghitalab, V. Mottaghitalab, and M. Farokhi, *Fabrication of porous chitosan/poly (vinyl alcohol) reinforced single-walled carbon nanotube nanocomposites for neural tissue engineering.* Journal of biomedical nanotechnology, 2011. **7**(2): p. 276-284.

33. Stampella, A., A. Papi, G. Rizzitelli, M. Costantini, C. Colosi, A. Barbetta, M. Massimi, L.C. Devirgiliis, and M. Dentini, *Synthesis and characterization of a novel poly(vinyl alcohol) 3D platform for the evaluation of hepatocytes' response to drug administration.* Journal of Materials Chemistry B, 2013. **1**(24): p. 3083-3098.

34. Brownsey, G.J. and V.J. Morris, *Mixed and filled gels - models for foods*, in *Food structure : its creation and evaluation*, J.M.V. Blanshard and J.R. Mitchell, Editors. 1988, Butterworths: London ; Boston. p. 7-14.

35. Leibinger, A., A. Forte, Z. Tan, M. Oldfield, F. Beyrau, D. Dini, and F. Rodriguez y Baena, *Soft Tissue Phantoms for Realistic Needle Insertion: A Comparative Study.* Annals of Biomedical Engineering, 2015: p. 1-11.

36. Miyashita, H., S. Shimmura, H. Kobayashi, T. Taguchi, N. Asano-Kato, Y. Uchino, M. Kato, J. Shimazaki, J. Tanaka, and K. Tsubota, *Collagen-immobilized poly(vinyl alcohol) as an artificial cornea scaffold that supports a stratified corneal epithelium.* J Biomed Mater Res B Appl Biomater, 2006. **76**(1): p. 56-63.

37. Gefen, A. and S.S. Margulies, *Are in vivo and in situ brain tissues mechanically similar?* J Biomech, 2004. **37**(9): p. 1339-52.

38. Zheng, Y.-P., A.F. Mak, and B. Lue, *Objective assessment of limb tissue elasticity: development of a manual indentation procedure.* Journal of rehabilitation research and development, 1999. **36**(2): p. 71-85.

39. van Dommelen, J.A.W., T.P.J. van der Sande, M. Hrapko, and G.W.M. Peters, *Mechanical properties of brain tissue by indentation: Interregional variation.* Journal of the Mechanical Behavior of Biomedical Materials, 2010. **3**(2): p. 158-166.

40. Fan, Z. and J.Y. Rho, *Effects of viscoelasticity and time-dependent plasticity on nanoindentation measurements of human cortical bone.* J Biomed Mater Res A, 2003. **67**(1): p. 208-14.

41. Chatelin, S., A. Constantinesco, and R. Willinger, *Fifty years of brain tissue mechanical testing: from in vitro to in vivo investigations.* Biorheology, 2010. **47**(5-6): p. 255-76.

42. Fedorov, A., R. Beichel, J. Kalpathy-Cramer, J. Finet, J.-C. Fillion-Robin, S. Pujol, C. Bauer, D. Jennings, F. Fennessy, and M. Sonka, *3D Slicer as an image computing platform for the Quantitative Imaging Network.* Magnetic resonance imaging, 2012. **30**(9): p. 1323-1341.

43. Rasin, I., Z. Pekar, O. Sadowsky, A. Forte, S. Galvan, D. Dini, M. Shoham, and L. Joskowicz. *Real-time modeling of intra-operative brain shift based on video tracking.* in *Proceedings of The Hamlyn Symposium on Medical Robotics.* 2014. London: GZ Yang and A Darzi.

44. Gamonpilas, C., M. Charalambides, and J. Williams, *Determination of large deformation and fracture behaviour of starch gels from conventional and wire cutting experiments.* Journal of materials science, 2009. **44**(18): p. 4976-4986.

45. Forte, A., F. D'Amico, M. Charalambides, D. Dini, and J. Williams, *Modelling and experimental characterisation of the rate dependent fracture properties of gelatine gels.* Food Hydrocolloids, 2015. **46**: p. 180-190.

46. Chun, Y.S. and W.N. Kim, *Thermal properties of poly(hydroxybutyrate-co-hydroxyvalerate) and poly(ϵ-caprolactone) blends.* Polymer, 2000. **41**(6): p. 2305-2308.

47. Kasapis, S., E.R. Morris, I.T. Norton, and C.R.T. Brown, *Phase equilibria and gelation in gelatin/maltodextrin systems — Part III: phase separation in mixed gels.* Carbohydrate Polymers, 1993. **21**(4): p. 261-268.

48. Ahrens, J., B. Geveci, and C. Law, *ParaView: An End-User Tool for Large-Data Visualization*, in *The Visualization Handbook*, C. Hansen and C. Johnson, Editors. 2005, Butterworth-Heinemann: Burlington. p. 717-731.

49. Hill, D.L., C.R. Maurer Jr, R.J. Maciunas, J.A. Barwise, M.J. Fitzpatrick, and M.Y. Wang, *Measurement of intraoperative brain surface deformation under a craniotomy.* Neurosurgery, 1998. **43**(3): p. 514-526.

50. Dorward, N.L., O. Alberti, B. Velani, F.A. Gerritsen, W.F. Harkness, N.D. Kitchen, and D.G. Thomas, *Postimaging brain distortion: magnitude, correlates, and impact on neuronavigation.* Journal of neurosurgery, 1998. **88**(4): p. 656-662.

51. Nimsky, C., O. Ganslandt, S. Cerny, P. Hastreiter, G. Greiner, and R. Fahlbusch, *Quantification of, visualization of, and compensation for brain shift using intraoperative magnetic resonance imaging.* Neurosurgery, 2000. **47**(5): p. 1070-1080.

52. Wang, T.-W. and M. Spector, *Development of hyaluronic acid-based scaffolds for brain tissue engineering.* Acta Biomaterialia, 2009. **5**(7): p. 2371-2384.

53. Garo, A., M. Hrapko, J.A. van Dommelen, and G.W. Peters, *Towards a reliable characterisation of the mechanical behaviour of brain tissue: The effects of post-mortem time and sample preparation.* Biorheology, 2007. **44**(1): p. 51-8.

54. Peters, G.W., J.H. Meulman, and A.A. Sauren, *The applicability of the time/temperature superposition principle to brain tissue.* Biorheology, 1997. **34**(2): p. 127-38.

55.   Hrapko, M., J.A. van Dommelen, G.W. Peters, and J.S. Wismans, *The influence of test conditions on characterization of the mechanical properties of brain tissue.* J Biomech Eng, 2008. **130**(3): p. 031003.

56.   Arbogast, K.B. and S.S. Margulies, *Regional differences in mechanical properties of the porcine central nervous system.* 1997, SAE Technical Paper.

57.   Vappou, J., E. Breton, P. Choquet, C. Goetz, R. Willinger, and A. Constantinesco, *Magnetic resonance elastography compared with rotational rheometry for in vitro brain tissue viscoelasticity measurement.* Magnetic Resonance Materials in Physics, Biology and Medicine, 2007. **20**(5-6): p. 273-278.

58.   Miya, M., R. Iwamoto, and S. Mima, *FT-IR study of intermolecular interactions in polymer blends.* Journal of Polymer Science: Polymer Physics Edition, 1984. **22**(6): p. 1149-1151.